Accepted Manuscript

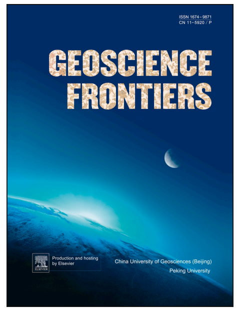

Raman-IR vibrational and XRD characterization of ancient and modern mineralogy from volcanic eruption in Tenerife Island: Implication for Mars

E.A. Lalla, G. López-Reyes, A. Sansano, A. Sanz-Arranz, J. Martinez-Frías, J. Medina, F. Rull-Pérez

PII: S1674-9871(15)00088-2

DOI: 10.1016/j.gsf.2015.07.009

Reference: GSF 377

To appear in: *Geoscience Frontiers*

Received Date: 18 November 2014

Revised Date: 28 July 2015

Accepted Date: 31 July 2015

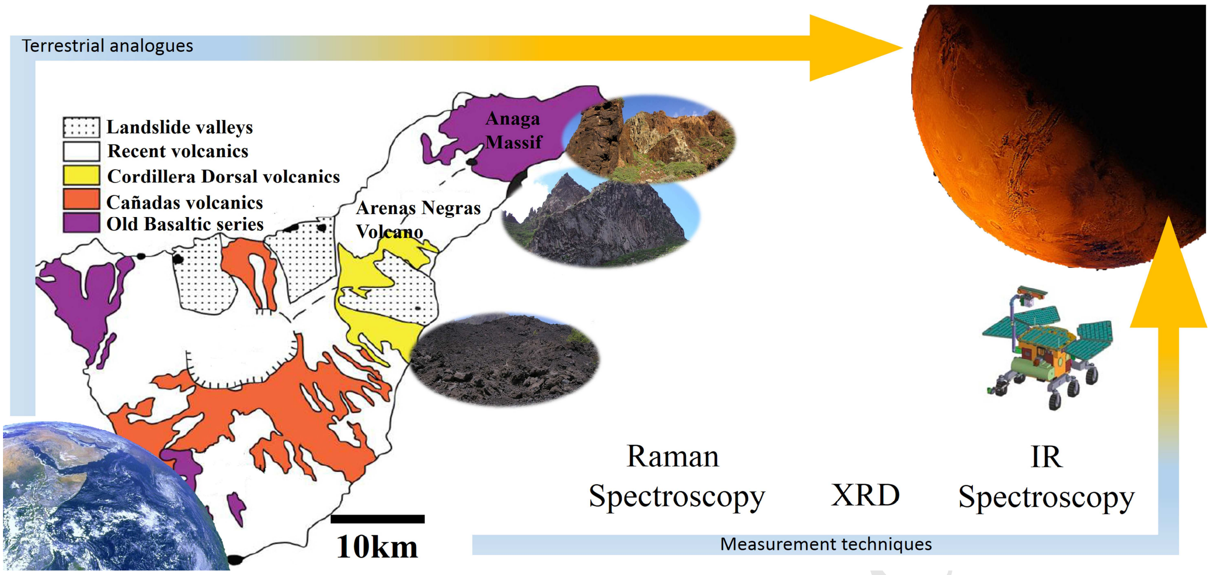

Terrestrial analogues
Landslide valleys
Recent volcanics
Cordillera Dorsal volcanics
Cañadas volcanics
Old Basaltic series
Anaga Massif
Arenas Negras Volcano
10km
Raman Spectroscopy
XRD
IR Spectroscopy
Measurement techniques

Raman-IR vibrational and XRD characterization of ancient and modern mineralogy from volcanic eruption in Tenerife Island: Implication for Mars

E. A. Lalla[a,b,*], G. López-Reyes[b], A. Sansano[b], A.Sanz-Arranz[b], J. Martinez-Frías[c], J. Medina[b], F. Rull-Pérez[b].

[a]Department of Physics, Faculty of Science, University of La Laguna, San Cristobal de La Laguna, Santa Cruz de Tenerife, CP 38206, Spain.

[b] Unidad Asociada al Centro de Astrobiología CSIC-INTA associated to the NASA Astrobiology Center – Instituto Nacional de Técnica Aeroespacial, Torrejón de Ardoz, CP 28850, Madrid, Spain.

[c]Department of Earth Dynamics and Observation , Instituto de Geociencias IGEO-(CSIC-UCM), Facultad de Ciencias Geológicas, Ciudad Universitaria, CP 28040, Madrid, Spain

*Corresponding author. E-mail: lallaea@cab.inta-csic.es, emmanuellalla@gmail.com

ABSTRACT

A detailed vibrational Raman-IR spectroscopic and diffractional analyses have been performed on basalts from two locations from Tenerife Island: (1) the Arenas Negras volcano which belongs to the historical eruption not showing visible alteration and (2) Pillow Lavas zone from Anaga Massif which shows a clearly fluid-rock interaction caused by submarine alteration. These places have been extensively studied due to its similarity with the surface of Mars. The analysis is based on the mineral detection of selected samples by a Micro-Raman study of the materials. The complementary techniques have confirmed the mineralogy detected by the Raman measurement. The results show a volcanic environment behavior with primary phases like olivine, pyroxene, and feldspar/plagioclase. Moreover, the presence of accessory minerals or secondary mineralization like phosphate, iron oxides, zeolite or carbonates shows the alteration processes on each outcrop. Moreover, the variation in the crystallinity and amorphous phases is related to fluid-rock interaction caused by hydrothermal episodes and external weathering processes, which shows several analogies with the ancient volcanic activity from Mars.

Keywords: Mars, Volcanoes, Terrestrial Analog, Raman Spectroscopy, Tenerife Island, mineralogy.

1. INTRODUCTION

Nowadays, Raman spectroscopy is considered one of the next generation techniques for planetary exploration due to its multiple advantages. Among others, Raman spectroscopy is a non-destructive analytical tool, capable of obtaining vibrational, rotational and other low-frequency modes information of the selected target (Rull-Pez and Martinez-Frias, 2006; Courres-Lacoste et al., 2007). One of the cutting edge research field applications for the Raman technique is the planetary science, where several instruments are being developed such as the Scanning Habitable Environments with Raman & Luminescence for Organics and Chemicals Instrument on NASA (SHERLOC) or SuperCam on NASA-France consortium for the NASA mission in 2020 (Grossman, 2013; Campbell et al., 2015). On the other hand, the next European mission to Mars, the ESA-ExoMars rover mission on 2018, will be equipped with a Raman Laser Spectrometer (RLS) as part of the analytical suite in the body of the vehicle (Rull-Pez and Martinez-Frias, 2006; Courres-Lacoste et al., 2007; Bost et al., 2015). The main applications of this instrument are focused on the exobiological and geochemical targets. Thus, the RLS is capable to detect different mineral phases, establishing the main mineralogical sequences and following secondary ones such as carbonates, sulfates and hydrated minerals formation (Edwards et al., 2004; Rull-Pez and Martinez-Frias, 2006; Lalla et al., 2010; Bost et al., 2015). The research and technical progress behind the Raman instrument is of fundamental importance for the future success. In this regard, it is important to highlight the appropriate preparation of the prototypes, the calibration, the realistic measurement conditions, the spectroscopic characterizations of natural samples and mineral species. Thus, it is necessary to analyze different Martian analogue materials, terrestrial analogues and different outcrops that will allow scientists to obtain ground accurate information of past and present of Mars (Bost et al., 2013, 2015).

The views of young volcanos and their volcanic features provided, such as Hawaii or Galapagos Island, show that the diversity of volcanic landscapes, size of lava flow fields, the dimensions of volcanic channels and the mode of emplacement of deposits may relate similarities with volcanos on the red planet. In this regards, the Viking Orbiter, Apollo, Voyager, and Magellan images can be inferred and confirm it (Xiao et al., 2012; Graham et al., 2015). From the geochemical point of view, the results enforces these considerations when the data received from NASA missions (MER and Curiosity-MSL) is compared (Kuhn, 2015). Apart from the Hawaiian Islands, the Canaries Island are one of the most interesting oceanic islands in the world for carried volcanic and geophysical research considering the geological complexity and heterogeneity in the Archipelago formation (Carracedo, 1999; Parthasarathy et al., 2003; Galindo et al., 2005). Furthermore, special attention has been done on the Tenerife Island, where multiple types of extrusive structure, petrological and geochemical variability are also present. In this regards, 20 million years of volcanism can be recognized on the Tenerife Island due to the volcanoes remains emergent until mass-wasting is completed. These features added to the gravitational general collapses and different erosion processes increase the interest for deeper studies (Carracedo, 1999; Acocella, 2007) in the fields of analogy with the Martian volcanology (Lalla et al., 2010; Lalla, 2014). For this research the two zones chosen present different primary and secondary mineralogy where alteration processes and rock/fluid interactions are present (marine, hydrothermal and meteoritic water). Thus, Tenerife geology presents all major conditions for becoming a Martian volcanic analogue, due to the geological complexity and heterogeneity of the volcanic surface are similar to Mars. In this regard, the geo-diversity of the two terrestrial analogues is useful for the evaluation of analytical conditions, the pre-selection of appropriate target sites, sampling and site characterization strategies for overall mission operations (Bishop et al., 2004; Farr, 2004; Leill? 2009; West and Clarke, 2010; Prinsloo et al., 2011). The main motivation of this research is to obtain a complete spectral mineralogical analysis of two volcanic outcrops (the Arenas Negras volcano and the Pillow Lavas zones) by Raman spectroscopy and presenting its mineralogical analogies with the ancient volcanic activity of the Martian planet. In this regard, a complete spectral mineralogy analysis from potential models could be used for the understanding of original unaltered material on Mars. In addition, the combination of Raman spectroscopy with X-Ray diffraction, IR- spectroscopy and SEM Microscopy help us to confirm the Raman information and provide complementary information for the characterization of the mineralogy detected.

2. MATERIALS AND METHODS

2.1 Geological target description and sampling

The selected places for the research have been considered especially by the geological eruptional period on the Tenerife Island. The first zone is placed on the Anaga massif (Fig. 1). It has been selected due to the submarine hydrothermal and weathering processes occurred on the outcrop. Moreover, the Pillow Lava formation is an unequivocal sign of volcanism on aqueous environment and, likely, the most abundant structural type on Earth (Ancochea et al., 1990) being the base of the island underneath the sea and the first part of the island formation. In this formation time, the volcanic activity was more violent due to the combination of water, gas eruptions and magma surrounding activities, giving the possibility to create peculiar geological fragments considering the geochemistry and mineralogy. The studies of these geological outcrops indicate an igneous material with the explained origin. They were formed primary by a basinitic composition from “8 Ma”, alkali basalt around from “5.8 Ma” and basinitic activity from “4.2 Ma”, with the existence of fossil hydrothermal systems and the existence of Fe-rich silica amorphous phase alteration to a groundmass of celadonite and opaline mixture rich in Fe-(hydro) oxides (Bustillo and Martez-Frs, 2003; Thirlwall et al., 2000). The selection of this outcrop for planetary implications is due to similar possible lava deposits have been reported on Mars, which have similar geomorphology to the terrestrial Tuyas (Leverington, 2011; Martez-Alonso et al., 2011), where exist the possibility of Pillow Lavas formed by the past water activity on Mars. The samples were collected from the Igueste ravine at an altitude of eighty six meters, located at (*28º32’06”N, 16º09’24”W)* near the southern coast of Anaga massif in 2009.

The second area, named as the Arenas Negras volcano (Fig. 1), dates back to one of latest eruptions from Tenerife (ca. 400 years ago), which belongs to the triple eruption of 1704–1705 (“Siete Fuentes”, “Fasnia” and “Arenas Negras”). It is worth to note that the samples are minimally affected by the meteoritic water and other external hydrothermal process (Solana, 1996; Lalla, 2014). The volcanic material belongs to AA lava type, composed by pyroxene-olivine with idiomorphic phenocrystals (millimeter size). The olivine is forsterite and the clino-pyroxene is augite (Solana, 1996). The matrix is composed by micro-crystals of plagioclase, augite, olivine and idiomorphic opaque of different sizes (Hernandez et al., 1993; Lalla et al., 2010). However, the secondary alteration could be caused either by the water vapors trapped within the pores of the glass particles creating alteration material under closed-system conditions or by weathering process (Hernandez et al., 1993; Villasante-Marcos et al., 2014). The sample set was collected by picking out samples on the studied areas during several expeditions in 2010, being all of them catalogued and photographed (Fig. 1). In the case of the Arenas Negras volcano, thirteen samples were collected from three different zones: 3 from the first zone TNFG01 (*28º19'53" N, 16º22'34" W)*; six from the second zone TNFG02 *(28º19'44" N, 16º25'39" W)* and two from the third zone TNFG03 (*28º19'44" N, 16º25'39" W)*. The selection of the zone has been done taking in consideration the volcanic crater (TNFG03), the middle zone (TNFG02) and the end of lava eruption (TNFG01) and eruption time. In this regard, the magma accumulation at the crater has a 8–10 m thick being the last days of the eruption (TNFG03). On the other hand, the TNFG03 zone corresponds to the beginning of the eruption where the distal part has a thickness of 2–3 m. The eruption distance has 9 km along the Güimar Valley where the water alteration by weathering is increased with the distance.

2.2 Experimental setup and Conditions:

The micro-Raman mineralogical characterization of the samples was performed with a microscope Nikon Eclipse E600 coupled to a spectrometer KOSI Holospec f/1.8i with best resolution of 5 cm^{-1}, illuminated by a laser REO LSRP-3501 He-Ne 632.8 nm. The detection was performed by a CCD Andor DV420A-OE-130. The laser power used was 14 mW with a spot diameter of 15 μm and the Raman mapping of the bulk surface of the sample was done by the Micro-Raman Prior Proscan II motorized stage in automatic mode in order to detect the different mineralization. However, the optimum recording conditions were obtained by varying the laser power, microscope objective and the confocal spot size (XY instrument) as required for the different samples. The spectra were directly acquired on the sample material without any sample preparation. The FT-Raman analysis was performed with a Fourier Transform Raman (FT-Raman) Bruker

RSF 100/S, which allows the analysis of high fluorescence samples, making it is more suitable for some samples than the visible Raman equipment. The FT-Raman spectrometer is composed by a Nd:YAG Laser at 1064 nm, spectrograph with spectral range 851–1695 nm (NIR) and best spectral resolution of 2 cm^{-1}. The detector is a Bruker CCD model D418T cooled by liquid N_2. The working conditions achieved a spectral resolution of 4 cm^{-1} and a diameter spot of 100 µm approximately.

The X-ray diffraction analyses were carried out with a XRD diffractometer Philips PW1710 equipped with automatic divergent slit graphite monochromator and Cu-anode. Experimental conditions: CuKα radiation, λ = 0.154nm, a niquel filter, an aluminum sample-holder, 40 kV generator voltage, generator current 30 mA with a relation intensity of 0.5 (α_1/α_2) and angle range (2θº) from 5 to 70º. The Terra XRD diffractometer instrument based on the MSL-CheMin concept with a detector (1024 X 256 pixels) 2D peltier cooled CCD camera for XRD with a source cobalt X-ray tube of 30Kv-300uA was also used. For the XRD analysis a preparation was necessary, consisting on the powdering of a minimum part of the samples (2–4 mg) and sieved with a granulometry lower than 150 µm.

The complementary analysis with scanning electron microscopy (SEM) was performed with an ESEM-Quanta 200F Microscope. For this analysis, no sample preparation was necessary and the measurements were directly performed on the bulk samples.

The infrared spectroscopic data were obtained by means of a Fourier Transform Infrared spectrometer with an attenuated total reflectance accessory (FTIR-ATR). The ATR-FTIR Pelkin Elmer Spectra 100 spectrometer system was equipped with a diamond ATR universal system, and the spectral range spans from 650 to 4000 cm^{-1} with 4 cm^{-1} spectral resolution. The samples used on these analyses were the same as the ones prepared for the XRD analyses.

3. RESULTS AND DISCUSSION

3.1 Raman spectroscopy results

Table 1 and Figs. 2 and 3 compile and summarize the mineral species and phases identified by Raman Spectroscopy on the two studied zones.

The olivine species detected on both sites correspond to a forsterite, clearly visible by the typical doublet band at 820 and 850 cm^{-1} in accordance with the literature (Chopelas, 1991). Also, the detected mineral species show other vibrational modes which are: (1) the lattice mode of the olivine, both "translational and rotational" SiO_4 movements and the translational motions of the cations (Mg^{2+}, Fe^{2+}) in the crystal lattice at the zone below 400 cm^{-1}; (2) the internal bending vibrational modes of the SiO_4 ionic group at the region 400–700 cm^{-1}; and (3) the internal stretching vibrational modes of the SiO_4 ionic group at the 700–1000 cm^{-1} region (Kuebler et al., 2006). On the basis of theoretical modeling, it has been demonstrated that the high frequency peaks of the olivine are originated from a mixing of symmetric and anti-symmetric stretching modes of SiO_4 units (Piriou and McMillan, 1983; Lam et al., 1990). In this regard, the doublet at 820–850 cm^{-1} are the most intense peaks on the olivine Raman spectra. These peaks are used to identify the olivine in the multi-phase spectrum due to the fact that the relative peak height of the doublet is function of crystal orientation. In other words, it serves as a calibration method for chemical, compositional and structural characterization of this kind of mineral species (Kuebler et al., 2006; Mouri and Enami, 2008; Yasuzuka et al., 2009). The calibration method proposed by several author (Kuebler et al., 2006; Yasuzuka et al., 2009) has been applied on the samples collection and the results point to an forsterite-olivine behaviour detailed on Table 2. Nevertheless, compared to the Arenas Negras volcano, the Pillow Lava zone presents weak/poor results caused by an insignificant detection of olivine, which have been probably altered by the hydrothermal process on the submarine pillow lava formation. Thus, the $Mg^{\#}$=Mg/(Mg+Fe) estimation method is very sensitive to the pressure, the composition and the alteration process (Kuebler et al., 2006; Mouri and Enami, 2008).

Concerning to the pyroxene mineral species, the Raman technique shows the existence of diopside and augite. Moreover, the analyses of the spectral pattern, developed by other authors (Wang et al., 2001), taking into account the empirical rules and spectral convention enforces the previous results. Special attention has been paid to the following regions: (1) the 1100–800 cm^{-1} region (where the strong asymmetric peak at 1000 cm^{-1} approximately and some wide and weak peaks on its two wings caused by the $Si\text{-}O_{nbr}$ stretching are found); (2) the 800–600 cm^{-1} region (with a strong doublet or an asymmetric single peak near to 660 cm^{-1} due to the $Si\text{-}O_{br}$ stretching); (3) the 600–450 cm^{-1} region with a group of peaks which overlap each other, being of middle intensity and which correspond to the O-Si-O bending; (4) the 450–300 cm^{-1} region formed by overlapped strong peaks caused by a M-O stretching and M-O bending; and (5) some peaks of moderate intensity found below 300 cm^{-1} (Wang et al., 2001) . A detailed comparison of the intensity or the FWHM (Full Bandwidth at Half Maximum) of the principal bands has been performed for the different spectral regions detailed on Table 3. This comparison reveals that Pillows Lavas zone samples have a more amorphous behavior and possibly a more disordered structure than the Arenas Negras volcano samples provoked by the submarine hydrothermal activity and the possible overlapping of other mineral species (Huang et al., 2000; Wang et al., 2001; Prinsloo et al., 2011). On the Marion Island, the results shows a similar behavior of glassy phase systems (Prinsloo et al., 2011) and the main cause is the rapid cooling of the lava extrudes from a volcano, without a correct crystal growing. In the case of submarine alteration, the melting point of the crystal formation is decreased, increasing the obsidian glass formation. On the other hand, the calibration method developed by other authors (Huang et al., 2000; Wang et al., 2001), considering Mg/(Mg+Fe+Ca) relative concentration, where a relative change in the position of the peaks at 327 cm^{-1} and at 665 cm^{-1} has been applied (Table 3). For the Arenas Negras samples, the Mg/(Mg+Fe+Ca) value is approximately "0.4 ± 0.1" while it is "0.5 ± 1" for the Pillow Lava zone. This corresponds to a diopside-augitie behavior (Huang et al., 2000; Wang et al., 2001) .

The tectosilicate groups detected on the target outcrop are a plagioclase series between labradorite and andesine in the Pillow Lava zone and a plagioclase series (albite-oligoclase)- K-feldspar (albite-anorthoclase) on the Arenas Negras volcano. However this depends upon the sample under analysis. The detailed identification on the Raman spectral pattern was achieved by the spectral region method, where the strongest vibrational bands are produced by the structure of SiO_4 of tectosilicate group and located below 600 cm^{-1} (Freeman et al., 2008). Thus, special consideration has been taken for the characteristic triplet or doublet bands, located on the 450–515 cm^{-1} region where the strongest peak is at 505–515 cm^{-1}. Moreover, other vibrational regions have been considered for the correct mineral identification such as the 200–400 cm^{-1} zone which corresponds to the rotational-translational modes; the 600–800 cm^{-1} spectral zone, where the Raman modes are produced by the deformation modes of the tetrahedral; and the 900–1200 cm^{-1} region, where the vibrations are assigned to the vibrational stretching mode of the tetrahedral structure (Freeman et al., 2008).

Hematite has been detected both on Pillow Lava zone and the Arenas Negras volcano (Figs. 2a and 3a). Hematite is the most common Fe-oxide in nature, and it presents a polymorph structure caused by the high thermodynamics stability. The most important bands are: the vibrations at 221 and 490 cm^{-1} caused by an A_g mode; the vibrations at 245, 295, 305, 410 and 607 cm^{-1} being assigned to an E_g mode; and the broad peaks at 1323 cm^{-1} is caused by the magnons effects (Jubb and Allen, 2010). On the other hand, magnetite (Fe_2O_3) has also been detected on both zones, where the most intense peak of this oxide structure is found at 660 cm^{-1} and it can be assigned to the A_{1g} symmetry mode, while the other two peaks detected correspond to the F_{2g} mode at 550 and 504 cm^{-1} (Rull et al., 2007; Jubb and Allen, 2010). The analyses of the spectral patterns show that the Arenas Negras volcano presents a more crystalline behavior than the Pillow Lava zone. Furthermore, the concentration of hematite/magnetite is bigger on the Arenas Negras volcano than in the Pillow Lava zone which could be explained by the Fe^{2+} and the Fe^{3+} cations incorporation in other crystalline solution/mineral species caused by the hydrothermal alteration on the submarine processes.

The carbonate detected on the samples is calcite, very commonly found as a secondary product from hydrothermal alteration in the modern Earth system. The Raman vibrations in the carbonates can be obtained from the vibration of the $(CO_3)^{2-}$ internal modes, the vibration of hydroxyl molecules and the vibration modes M-O from the interactions between cations and O of either $(CO_3)^{2-}$, external or lattice modes. The most intense vibrations are the symmetric stretching of CO_3 at 1086 cm^{-1}; the symmetric bending of CO_3 at 715 cm^{-1}; and the external vibration of CO_3^- at 285 cm^{-1} (Rull et al., 2004; Rividi et al., 2010). It is necessary to quote that the signal was very low and sloped in comparison with other mineral species such as the pyroxene and olivine on the Pillow Lava zone. On the other hand, in the Arenas Negras volcano, the calcite was detected in conjunction with zeolite (Urmos et al., 1991; Hernandez et al., 1993). Moreover, a method, developed by Rull et al (Rull-Perez and Martinez-Frias, 2003), has been applied for obtaining the paragenesis of the mineral species. The analysis of measured parameters such as intensity and FWHM of the main peaks at 1086, 715 and 280 cm^{-1} converge to a magmatic formation in both sites (Rull-Perez and Martinez-Frias, 2003). The structure of hydrotalcite states that there is a broad range of compositions depending on cations. However, on the Anaga Pillow Lavas zone, the measurements show only a Raman vibration at 1060 cm^{-1}, which is caused by the combination of symmetric and antisymmetric stretching of the CO_3^{-}. Nevertheless, more peaks are necessary to perform an identification of the specific hydrotalcite species (Moroz et al., 2001; Frost et al., 2005). Concerning to the paragenesis, the rock/fluid interaction with submarine water is clearly the main cause of formation.

The calcium phosphate detected on the Arenas Negras volcano corresponds to an apatite structure, from which several Raman and IR active modes like the $PO^{3-}{}_4$, OH^- and $CO^{2-}{}_3$ active modes have been measured (Mooney et al., 1968; Antonakos et al., 2007;). The T_d symmetry of the $PO^{3-}{}_4$ vibrational mode creates the stretching mode A_1 at 960 cm^{-1} zone, the doubly degenerated bending E mode at 420 cm^{-1}, the triply degenerated anti-symmetric stretching mode F_2 at 1017 cm^{-1} and the triply degenerated bending F_2 at 567 cm^{-1} (Ohea et al., 1974; Cooney et al., 1999; Antonakos et al., 2007; Hill and Jha, 2007; Zattin et al., 2007).

The zeolites from the Arenas Negras volcano samples are abundant in the vesicular tops and bottoms of the basalt flows and flow breccias. The detailed classification of the zeolite performed by the Raman based classification technique determinates that it is a phillipsite. The spectra have been compared with different Raman spectral data from zeolite obtained from Raman online database such as RRUFF. Moreover, the vibrations at 420 and 480 cm^{-1} have been compared with the reference (Pechar, 1981), being in agreement with other authors (Gatta et al., 2010).

3.2 X-Ray diffraction analysis

The qualitative mineralogical analysis was performed based on the peak positions and its comparison with other standard patterns on the Fig. 4. For the analysis of different phases in multiphase specimens, the commercial software Phillips PW-1876 Pc-identify was used, which compares peak intensities attributed to the identified phases. These analyses reveal the existence of tectosilicates (plagioclase and K-feldspar), pyroxene (diopside or augite possibly) and olivine (forsterite) lines. Moreover, it is important to mention the existence of hematite and magnetite in a lower proportion for both analyzed zones. Nonetheless, the results are in agreement with the Raman analyses verifying the principal mineral phases.

3.3 ATR-FTIR analysis

The ATR-FTIR complementary analysis only shows the most intense vibration of Al-silicates at 1630 cm^{-1} and silicates at 1000 cm^{-1} in the mixture (Fig. 5). The main problem is that the minor mineral phases are masked by the host matrix mineral phases when crushed and mixed, and these cannot be detected in the spectra due to a relatively high detection threshold inherent to this kind of technique. However, IR-Spectroscopy is a very sensitive technique to the hydrogen bonding of the OH^- at 3300 cm^{-1} and the water vibration at 3600 cm^{-1} (Nakamoto, 1978; Rull et al., 2004). This feature plays an important role in determining the aqueous mineral identification in natural samples, which could be consequence of the rock-water interaction. As a result, the presence of Al-OH species, OH^- bands and H_2O vibrations can be confirmed (Nakamoto, 1978). The results could point to the hydration of the groundmass, caused either by the action of percolating water in the subaerial environment (the Arenas Negras volcano) or the action of the sea water in the case of the submarine environment (Pillow Lava zone).

3.4 SEM analysis

The results of SEM show the ubiquitous occurrence of the zeolites (phillipsite), which were only found in the many cavities of the rock, whose abundance and size are variable, forming radiating clusters with minor quantities of calcite (Fig. 6). The results are in agreement with the literature, the phillipsite has been identified by direct comparison to other SEM photograph, where similar alteration processes have occurred (Hernandez et al., 1993; Gatta et al., 2010;).

3.5 Discussions of the results

The mineralogy detected by the different techniques is summarized in Table 4. On the different outcrop, the mineral species detected correspond to a primary and secondary mineralization. The Pillow Lava zone has been submitted from the first processes of the island formation compared to the Arenas Negras volcano. The secondary minerals detected correspond to different variety of origins such as hydrothermal process or submarine processes. However, the mineralogy on the Arenas Negras volcano presents several similarities, despite the spectral differences on the Raman analysis.

The olivine is forsterite on the different zones, being in agreement with the references. On the other hand, the pyroxene detected are diopside-augite and considering the Raman detailed analysis, the spectral differences correspond to the broadening band which could be related to the submarine alteration or the overlapping on the mineral detection. The feldspar and plagioclase on the host matrix was detected by Raman spectroscopy and confirmed afterward through the two complementary technique (X-Ray diffraction and Infrared spectroscopy). Their composition varies depending on the samples and zones and this is indicative that the different cation content is conditioned by the local environment (temperature of formation and cooling rates). Furthermore, it causes a discontinuous Bowen series reaction in some cases (Haldar and Tijar, 2014). In the case of the oxides, they were detectable only by Raman spectroscopy and XRD, the

Pillow Lava outcrop presents less quantity detection compared to the Arenas Negras volcano. In this regard, the Fe is incorporated in other solid crystalline solution and glass by the submarine alteration.

The calcite presents a hydrothermal volcanic origin taking into account the Raman analysis of the spectra. The apatite corresponds to a volcanic accessory mineral, however it could be attributed to a contamination from submarine sediment (Pillow Lavas) or biological contamination (the Arenas Negras volcano) (Prinsloo et al., 2011).

The zeolite was detected only by Raman spectroscopy and confirmed by SEM. The origin of this mineral specie is clearly hydrothermal. The lava in the historical eruptions extruded with a big amount of water vapors at the south of Tenerife and it probably reacts fast with volcanic glasses at high temperatures in a closed-system (Hernandez et al., 1993; Rodruez et al., 2015). Therefore, the detected zeolite crystals has been originated by a similar hydrothermal process such as the Deccan Trap outcrop in India, where the glass is hydrated and dissoluted with the subsequent nucleation and growth of the zeolite (Hernandez et al., 1993; Parthasarathy et al., 2003; Parthasarathy and Sarkar, 2014). Also, several authors have obtained this zeolite phase by hydrothermal processes of synthetic water free glasses of some compositions by P-T-t (Pressure-Temperature close system) close system using distilled water at 200/250ºC and 4–5 weeks being in agreement with the natural result found on the outcrop (Ghobarkar et al., 2003; Parthasarathy et al., 2003; Parthasarathy and Sarkar, 2014;).

On the Table 4 is also presented a mineral comparison with the mineral detected on Mars considering the references (Bishop et al., 2004; Chevrier and Math, 2007; Bish et al., 2013; Wang et al., 2015). The mineral comparison have been considered the results from the analysis from Martian meteorites and Rover analysis. In this regard, the analysis from the Tenerife selected outcrops present similar mineral detection such as the Crater Gusev's mineralogy (Rice et al., 2010; Bish et al., 2013). Moreover, the Gale crater shows signatures of feldspar, pyroxene, magnetite and olivine. Also the data shows indication of phyllosilicate in the presence of basanites and a minor amount of sulfates (Bish et al., 2013). Concerning to the alteration minerals such as zeolite, they have been detected on the dust by orbiters (Ruff, 2004; Wray et al., 2009). As it can be observed, the mineralization presented on the outcrop and the compared with the Martian shows that the analogues present similar types of mineral origin: evaporitic process, water alteration, hydrothermalism and weathering (Chevrier and Math, 2007)). Moreover, future field-testing of the portable instrumentation and analysis of resulting multispectral with other analytical techniques (XRD and IR) have shown to be valuable, including the identification of spectral and synergy working of the Raman instrumentation with other techniques for planetary research. Also, the Raman data can reveal overall outcrop mineralogy and mineral structure, being a crucial factor in the selection of drill targets and interpretation of the local geology.

4. CONCLUSSIONS

Different samples from Pillow Lava zone from Anaga zone and the Arenas Volcano were characterized and studied by Raman spectroscopic techniques and several laboratory complementary techniques for the very first time, through a complete analysis of the mineralogy from the selected materials. Crystalline primary phases such as olivine, pyroxene, oxide, feldspar; and secondary minerals like carbonate, zeolite and phosphate have been confirmed by Raman spectroscopy and in some case confirmed by complementary methods detailed along this paper. Also, other amorphous/glassy materials, resulting from the hydrothermal alteration and weathering, were detected.

The crystalline phases of mineral species described along the paper are similar to those reported on materials of other volcanic terrestrial analogues and Mars observations. However, the samples present some differences on the secondary mineral species, such as the zeolite. The possibility to distinguish the zeolite by Raman spectroscopy helps us to deduce the rock-process formation or rock-process alteration. Thus, the enlargement of knowledge on terrestrial analogues helps on the planetary research with astrogeological implications, specially focused on the development of future Martian missions.

It has been shown that Raman spectroscopy on the altered igneous rocks is capable of detecting minor mineral phases which can be used to correlate the spectra with the cooling rate and temperature formation of the rocks, becoming a very useful technique for in-situ planetary exploration. Thus, the results reveal that Raman techniques are powerful and robust systems for the detection of aqueous processes and support the continued endeavors to use the Raman spectroscopy for Mars exploration. The combination of complementary (IR, XRD and SEM) techniques with Raman allows us to obtain comprehensive information about the mineralogy and to interpret the future information to be received from the solid solution structure on the Martian surface.

ACKNOWLEDGEMENTS

The work was supported by the MICINN with the Project AYA-2008-04529 for the development of the Raman-LIBS combined spectrometer for the ESA-ExoMars Mission. E. Lalla wish to thank MICINN for the FPI grants (BES-2009-024992).

REFERENCES

Acocella, V., 2007. Understanding caldera structure and development: An overview of analogue models compared to natural calderas. Earth-Science Rev. 85, 125–160. doi:http://dx.doi.org/10.1016/j.earscirev.2007.08.004

Ancochea, E., Fuster, J., Ibarrola, E., Cendrero, A., Coello, J., Hernan, F., Cantagrel, J.M., Jamond, C., 1990. Volcanic evolution of the island of Tenerife (Canary Islands) in the light of new K-Ar data. J. Volcanol. Geotherm. Res. doi:10.1016/0377-0273(90)90019-C

Antonakos, A., Liarokapis, E., Leventouri, T., 2007. Micro-Raman and (FTIR) studies of synthetic and natural apatites. Biomaterials 28, 3043–3054. doi:http://dx.doi.org/10.1016/j.biomaterials.2007.02.028

Bish, D.L., Blake, D.F., Vaniman, D.T., Chipera, S.J., Morris, R. V, Ming, D.W., Treiman, A.H., Sarrazin, P., Morrison, S.M., Downs, R.T., Achilles, C.N., Yen, A.S., Bristow, T.F., Crisp, J.A., Morookian, J.M., Farmer, J.D., Rampe, E.B., Stolper, E.M., Spanovich, N., Team, M.S.L.S., 2013. X-ray Diffraction Results from Mars Science Laboratory: Mineralogy of Rocknest at Gale Crater. Sci. 341 . doi:10.1126/science.1238932

Bishop, J.L., Murad, E., Lane, M.D., Mancinelli, R.L., 2004. Multiple techniques for mineral identification on Mars: a study of hydrothermal rocks as potential analogues for astrobiology sites on Mars. Icarus 169, 311–323. doi:http://dx.doi.org/10.1016/j.icarus.2003.12.025

Bost, N., Ramboz, C., LeBreton, N., Foucher, F., Lopez-Reyes, G., De Angelis, S., Josset, M., Venegas, G., Sanz-Arranz, A., Rull, F., Medina, J., Josset, J.-L., Souchon, A., Ammannito, E., De Sanctis, M.C., Di Iorio, T., Carli, C., Vago, J.L., Westall, F., 2015. Testing the ability of the ExoMars 2018 payload to document geological context and potential habitability on Mars. Planet. Space Sci. 108, 87–97. doi:10.1016/j.pss.2015.01.006

Bost, N., Westall, F., Ramboz, C., Foucher, F., Pullan, D., Meunier, A., Petit, S., Fleischer, I., Klingelhöfer, G., Vago, J.L., 2013. Missions to Mars: Characterisation of Mars analogue rocks for the International Space Analogue Rockstore (ISAR). Planet. Space Sci. 82–83, 113–127. doi:http://dx.doi.org/10.1016/j.pss.2013.04.006

Bustillo, M.A., Martínez-Frías, J., 2003. Green opals in hydrothermalized basalts (Tenerife Island, Spain): alteration and aging of silica pseudoglass. J. Non. Cryst. Solids 323, 27–33. doi:http://dx.doi.org/10.1016/S0022-3093(03)00288-6

Campbell, K.A., Guido, D.M., Gautret, P., Foucher, F., Ramboz, C., Westall, F., 2015. Geyserite in hot-spring siliceous sinter: Window on Earth's hottest terrestrial (paleo)environment and its extreme life. Earth-Science Rev. 148, 44–64. doi:10.1016/j.earscirev.2015.05.009

Carracedo, J.C., 1999. Growth, structure, instability and collapse of Canarian volcanoes and comparisons with Hawaiian volcanoes. J. Volcanol. Geotherm. Res. 94, 1–19. doi:http://dx.doi.org/10.1016/S0377-0273(99)00095-5

Chevrier, V., Mathé, P.E., 2007. Mineralogy and evolution of the surface of Mars: A review. Planet. Space Sci. 55, 289–314. doi:http://dx.doi.org/10.1016/j.pss.2006.05.039

Chopelas, A., 1991. Single crystal Raman spectra of forsterite, fayalite, and monticellite. Am. Mineral. 76, 1101–1109.

Cooney, T.F., Scott, E.R.D., Krot, A.N., Sharma, S.K., Yamaguchi, A., 1999. Vibrational spectroscopic study of minerals in the Martian meteorite ALH84001. Am. Mineral. 84, 1569–1576. doi:10.1016/0003-004X-99-0010-1569

Courrèges-Lacoste, G.B., Ahlers, B., Rull Perez, F., 2007. Combined Raman spectrometer/laser-induced breakdown spectrometer for the next ESA mission to Mars. Spectrochim. Acta Part A Mol. Biomol. Spectrosc. 68, 1023–1028. doi:http://dx.doi.org/10.1016/j.saa.2007.03.026

Edwards, H.G.M., Moody, C.A., Jorge Villar, S.E., Mancinelli, R., 2004. Raman spectroscopy of desert varnishes and their rock substrata. J. Raman Spectrosc. 35, 475–479. doi:10.1002/jrs.1170

Farr, T.G., 2004. Terrestrial analogs to Mars: The NRC community decadal report. Planet. Space Sci. 52, 3–10. doi:http://dx.doi.org/10.1016/j.pss.2003.08.004

Freeman, J.J., Wang, A., Kuebler, K.E., Jolliff, B.L., Haskin, L.A., 2008. Characterization of natural feldspars by raman spectroscopy for future planetary exploration. Can. Mineral. 46, 1477–1500. doi:10.3749/canmin.46.6.1477

Frost, R.L., Adebajo, M.O., Erickson, K.L., 2005. Raman spectroscopy of synthetic and natural iowaite. Spectrochim. Acta Part A Mol. Biomol. Spectrosc. 61, 613–620. doi:http://dx.doi.org/10.1016/j.saa.2004.05.015

Galindo, I., Soriano, C., Martí, J., Pérez, N., 2005. Graben structure in the Las Cañadas edifice (Tenerife, Canary Islands): Implications for active degassing and insights on the caldera formation. J. Volcanol. Geotherm. Res. 144, 73–87. doi:10.1016/j.jvolgeores.2004.11.017

Gatta, G.D., Cappelletti, P., Langella, A., 2010. Crystal-chemistry of phillipsites from the Neapolitan Yellow Tuff. Eur. J. Mineral. doi:10.1127/0935-1221/2010/0022-2027

Ghobarkar, H., Schäf, O., Massiani, Y., Knauth, P., 2003. The Reconstruction of Natural Zeolites: A New Approach to Announce Old Materials by their Synthesis, Kluwer Aca. ed. Springer-Verlag New York Inc. doi:10.1007/978-1-4419-9142-3

Graham, L., Graff, T.G., Aileen Yingst, R., ten Kate, I.L., Russell, P., 2015. 2012 Moon Mars Analog Mission Activities on Mauna Kea, Hawaii. Adv. Sp. Res. 55, 2405–2413. doi:10.1016/j.asr.2015.01.024

Grossman, L., 2013. NASA urged to seek live Martians with 2020 rover. New Sci. 219, 9. doi:10.1016/S0262-4079(13)61775-3

Haldar, S.K., Tišljar, J., 2014. Chapter 4 - Igneous Rocks, in: Tišljar, S.K.H. (Ed.), Introduction to Mineralogy and Petrology. Elsevier, Oxford, pp. 93–120. doi:http://dx.doi.org/10.1016/B978-0-12-408133-8.00004-3

Hernandez, J.E.G., del Pino, J.S.N., Martin, M.M.G., Reguera, F.H., Losada, J.A.R., 1993. Zeolites in pyroclastic deposits in southeastern tenerife (Canary Islands). Clays Clay Miner. 41, 521–526. doi:10.1346/CCMN.1993.0410501

Hill, C.J., Jha, A., 2007. Development of novel ternary tellurite glasses for high temperature fiber optic mid-IR chemical sensing. J. Non. Cryst. Solids 353, 1372–1376. doi:http://dx.doi.org/10.1016/j.jnoncrysol.2006.10.061

Huang, E., Chen, C.H., Huang, T., Lin, E.H., Xu, J.A., 2000. Raman spectroscopic characteristics of Mg-Fe-Ca pyroxenes. Am. Mineral. 85, 473–479.

Jubb, A.M., Allen, H.C., 2010. Vibrational Spectroscopic Characterization of Hematite, Maghemite, and Magnetite Thin Films Produced by Vapor Deposition. ACS Appl. Mater. Interfaces 2, 2804–2812. doi:10.1021/am1004943

Kuebler, K.E., Jolliff, B.L., Wang, A., Haskin, L.A., 2006. Extracting olivine (Fo–Fa) compositions from Raman spectral peak positions. Geochim. Cosmochim. Acta 70, 6201–6222. doi:http://dx.doi.org/10.1016/j.gca.2006.07.035

Kuhn, N., 2015. Chapter 2 - Overview of Mars, in: Kuhn, N.B.T.-E. in R.G. (Ed.), Experiments in Reduced Gravity. Elsevier, Oxford, pp. 17–26. doi:http://dx.doi.org/10.1016/B978-0-12-799965-4.00002-9

Lalla, E., Caramazana Sansano, A., Sanz-Arranz, A., Alonso Alonso, P., Medina García, J., Martinez-frías, J., Rull-Perez, F., 2010. Espectroscopía Raman de Basaltos Correspondientes al Volcán de Las Arenas , Tenerife. MACLA - Soc. Española Mineral. 13, 129–130.

Lalla, E.A., 2014. Tenerife como análogo de Marte: Caracterización multianalítica (Raman, DRX, ATR-FTIR, SEM y MossBaeur) de muestras de interés planetario y astrobiológico. Dep. Física la Mater. Condens. Cristalogr. y Minerealogía - Univ. Valladolid. University of Valladolid.

Lam, P.K., Yu, R., Lee, M.W., Sharma, S.K., 1990. Structural distortions and vibrational modes in Mg2SiO4. Am. Mineral.

Léveillé, R., 2009. Validation of astrobiology technologies and instrument operations in terrestrial analogue environments. Comptes Rendus Palevol 8, 637–648. doi:http://dx.doi.org/10.1016/j.crpv.2009.03.005

Leverington, D.W., 2011. A volcanic origin for the outflow channels of Mars: Key evidence and major implications. Geomorphology 132, 51–75. doi:http://dx.doi.org/10.1016/j.geomorph.2011.05.022

Martínez-Alonso, S., Mellon, M.T., Banks, M.E., Keszthelyi, L.P., McEwen, A.S., 2011. Evidence of volcanic and glacial activity in Chryse and Acidalia Planitiae, Mars. Icarus 212, 597–621. doi:http://dx.doi.org/10.1016/j.icarus.2011.01.004

Mooney, R.W., Toma, S.Z., Goldsmith, R.L., Butler, K.H., 1968. Normal vibrations of the PO43− ion, site symmetry C3v, IN Sr3(PO4)2 and Ba3(PO4)2. J. Inorg. Nucl. Chem. doi:10.1016/0022-1902(68)80337-9

Moroz, T., Razvorotneva, L., Grigorieva, T., Mazurov, M., Arkhipenko, D., Prugov, V., 2001. Formation of spinel from hydrotalcite-like minerals and destruction of chromite implanted by inorganic salts. Appl. Clay Sci. 18, 29–36.

Mouri, T., Enami, M., 2008. Raman spectroscopic study of olivine-group minerals. J. Mineral. Petrol. Sci. 103, 100–104. doi:10.2465/jmps.071015

Nakamoto, K., 1978. Infrared and Raman Spectra of Inorganic and Coordination Compounds, Part A: Theory and Applications in Inorganic Chemistry, Sixth Edit. ed. John Wiley & Sons, Ltd.

O'Shea, D.C., Bartlett, M.L., Young, R.A., 1974. Compositional analysis of apatites with laser-raman spectroscopy:(oh,f,cl)apatites. Arch. Oral Biol. 19, 995–906. doi:http://dx.doi.org/10.1016/0003-9969(74)90086-7

Parthasarathy, G., Choudary, B.M., Sreedhar, B., Kunwar, A.C., Srinivasan, R., 2003. Ferrous saponite from the Deccan Trap , India , and its application in adsorption and reduction of hexavalent chromium. Am. Mineral. 88, 1983–1988.

Parthasarathy, G., Sarkar, P.K., 2014. High pressure temperature studies of phyllosilicates from the Deccan Trap: Implications to Martian Mineralogy and Near Subsurface Processes, in: Lunar and Planetary Science Conference. Houston, Texas, p. 1326. doi:10.1002/jgre.20161.

Pechar, F., 1981. Study of the Raman Polarization Spectra of the Single Crystal Phillipsite. Krist. und Tech. 16, 917–920. doi:10.1002/crat.19810160810

Piriou, B., McMillan, P., 1983. The high-frequency vibrational spectra of vitreous and crystalline orthosilicates. Am. Mineral.

Prinsloo, L.C., Colomban, P., Brink, J.D., Meiklejohn, I., 2011. A Raman spectroscopic study of the igneous rocks on Marion Island: A possible terrestrial analogue for the geology on Mars. J. Raman Spectrosc. 42, 626–632. doi:10.1002/jrs.2756

Rice, M.S., Bell, J.F., Cloutis, E.A., Wang, A., Ruff, S.W., Craig, M.A., Bailey, D.T., Johnson, J.R., de Souza, P.A., Farrand, W.H., 2010. Silica-rich deposits and hydrated minerals at Gusev Crater, Mars: Vis-NIR spectral characterization and regional mapping. Icarus 205, 375–395. doi:10.1016/j.icarus.2009.03.035

Rividi, N., van Zuilen, M., Philippot, P., Ménez, B., Godard, G., Poidatz, E., 2010. Calibration of Carbonate Composition Using Micro-Raman Analysis: Application to Planetary Surface Exploration. Astrobiology 10, 293–309. doi:10.1089/ast.2009.0388

Rodríguez, F., Pérez, N.M., Padrón, E., Melián, G., Piña-Varas, P., Dionis, S., Barrancos, J., Padilla, G.D., Hernández, P.A., Marrero, R., Ledo, J.J., Bellmunt, F., Queralt, P., Marcuello, A., Hidalgo, R., 2015. Surface geochemical and geophysical studies for geothermal exploration at the southern volcanic rift zone of Tenerife, Canary Islands, Spain. Geothermics 55, 195–206. doi:10.1016/j.geothermics.2015.02.007

Ruff, S.W., 2004. Spectral evidence for zeolite in the dust on Mars. Icarus 168, 131–143. doi:10.1016/j.icarus.2003.11.003

Rull, F., Martinez-Frias, J., Rodríguez-Losada, J.A., 2007. Micro-Raman spectroscopic study of El Gasco pumice, western Spain. J. Raman Spectrosc. 38, 239–244. doi:10.1002/jrs.1628

Rull, F., Martinez-Frias, J., Sansano, A., Medina, J., Edwards, H.G.M., 2004. Comparative micro-Raman study of the Nakhla and Vaca Muerta meteorites. J. Raman Spectrosc. 35, 497–503. doi:10.1002/jrs.1177

Rull-Perez, F., Martinez-Frias, J., 2003. Identification of calcite grains in the Vaca Muerta mesosiderite by Raman spectroscopy. J. Raman Spectrosc. 34, 367–370. doi:10.1002/jrs.1003

Rull-Pérez, F., Martinez-Frias, J., 2006. Raman spectroscopy goes to Mars. Spectrosc. Eur. 18, 18–21.

Solana, M.C., 1996. La erupción de 1704-1705 en Tenerife, Islas Canarias. Reconstrucción, peligros asociados y su mitigación. Geogaceta 20, 540–542.

Thirlwall, M.F., Singer, B.S., Marriner, G.F., 2000. 39Ar–40Ar ages and geochemistry of the basaltic shield stage of Tenerife, Canary Islands, Spain. J. Volcanol. Geotherm. Res. 103, 247–297. doi:http://dx.doi.org/10.1016/S0377-0273(00)00227-4

Urmos, J., Sharma, S.K., Mackenzie, F.T., 1991. Characterization of some biogenic carbonates with Raman spectroscopy. Am. Mineral.

Villasante-Marcos, V., Finizola, A., Abella, R., Barde-Cabusson, S., Blanco, M.J., Brenes, B., Cabrera, V., Casas, B., De Agustín, P., Di Gangi, F., Domínguez, I., García, O., Gomis, A., Guzmán, J., Iribarren, I., Levieux, G., López, C., Luengo-Oroz, N., Martín, I., Moreno, M., Meletlidis, S., Morin, J., Moure, D., Pereda, J., Ricci, T., Romero, E., Schütze, C., Suski-Ricci, B., Torres, P., Trigo, P., 2014. Hydrothermal system of Central Tenerife Volcanic Complex, Canary Islands (Spain), inferred from self-potential measurements. J. Volcanol. Geotherm. Res. 272, 59–77. doi:10.1016/j.jvolgeores.2013.12.007

Wang, A., Jolliff, B.L., Haskin, L.A., Kuebler, K.E., Viskupic, K.M., 2001. Characterization and comparison of structural and compositional features of planetary quadrilateral pyroxenes by Raman spectroscopy. Am. Mineral. 86, 790–806.

Wang, A., Korotev, R.L., Jolliff, B.L., Ling, Z., 2015. Raman imaging of extraterrestrial materials. Planet. Space Sci. 112, 23–34. doi:10.1016/j.pss.2014.10.005

West, M.D., Clarke, J.D.A., 2010. Potential martian mineral resources: Mechanisms and terrestrial analogues. Planet. Space Sci. 58, 574–582. doi:http://dx.doi.org/10.1016/j.pss.2009.06.007

Wray, J.J., Murchie, S.L., Squyres, S.W., Seelos, F.P., Tornabene, L.L., 2009. Diverse aqueous environments on ancient Mars revealed in the southern highlands. Geol. 37 , 1043–1046. doi:10.1130/G30331A.1

Xiao, L., Huang, J., Christensen, P.R., Greeley, R., Williams, D.A., Zhao, J., He, Q., 2012. Ancient volcanism and its implication for thermal evolution of Mars. Earth Planet. Sci. Lett. 323-324, 9–18. doi:10.1016/j.epsl.2012.01.027

Yasuzuka, T., Ishibashi, H., Arakawa, M., Yamamoto, J., Kagi, H., 2009. Simultaneous determination of Mg# and residual pressure in olivine using micro-Raman spectroscopy. J. Mineral. Petrol. Sci. 104, 395–400. doi:10.2465/jmps.090615

Zattin, M., Bersani, D., Carter, A., 2007. Raman microspectroscopy: A non-destructive tool for routine calibration of apatite crystallographic structure for fission-track analyses. Chem. Geol. 240, 197–204. doi:10.1016/j.chemgeo.2007.02.007

List of Figures

Figure 1. (A) Pictures of sampling zone of the Anaga massif and selected samples. (B) Simplified geological and topographic map of Tenerife illustrating the distribution of visible vents and the map of mafic emission centers and vent alignments on Tenerife Island. (C) Pictures and of sampling zone of "Las Arenas Negras volcano and selected samples, where is detailed the three zones-studied (Credits: Google). (D) Simplified scheme of the Tenerife formation: (1) Submarine eruptions (20–50 Ma); (2) ancient basaltic formation (7 Ma); (3) latest basaltic series-II, III, IV–(3 Ma); (4) gravitational slandslide (800 Ma.); and (5) valley formation and historical eruptions.

Figure 2. Raman spectra of the main phases recorded on the Arenas Negras volcano: (a) pyroxene, (b) forsterite, (c) apatite, (d) hematite, (e) plagioclases, (f) calcite and (g) zeolite + calcite.

Figure 3. Raman spectra recorded on the Pillow Lava main phases: (a) hematite + magnetite, (b) alteration magnetite, (c) magnetite, (d) hydrotalcite + organics, (e) plagioclase, (f) forsterite + pyroxene + calcite and (g) pyroxene.

Figure 4. XRD diffractograms of different selected samples. (a) Pillow Lava (sub-sample 1); (b) Pillow Lava (sub-sample 2); (c) Pillow Lava (sub-sample 3); (d) Las Arenas Negras Volcano (TNFG01); (e) Las Arenas Negras Volcano (TNFG02); (f) Las Arenas Negras Volcano (TNFG03). Mineral assignment: (●) Plagioclase, (■) Pyroxene, (✚) Hematite, (♦) Feldspar, (▲) Olivne and(▼) Goethite.

Figure 5. ATR-FTIR Infrared Spectra from Pillow Lava zone and the Arenas Negras volcano. The H_2O and OH^- vibration and the Al-OH silicate vibration bands can be

observed. (a-c) Pillow Lava (selected samples spectra) (d) TNFG01 sample and (e) TNFG03 sample.

Figure 6. SEM Photograph of the zeolite occurrence. Radiating cluster of the zeolite crystal inside the cavities from the Arenas Negras volcano (a) and (b).

Table1. Summary of crystalline inorganic phases detected by Raman spectroscopy on the Pillow Lava zone and the Arenas Negras volcano.

Characteristic (peaks/cm^{-1})	**Pillow Lava Zone**	**The Arenas Negras volcano**
821, 853	Olivine (Forsterite)	Olivine (Forsterite)
324, 358, 385, 663, 1004	Pyroxene (Diopside, Augite)	Pyroxene (Diopside, Augite)
280, 460/463, 480/485, 505	K-Feldspar/Plagioclase	K-Feldspar/Plagioclase
283, 712, 1087/1085	Carbonate (Calcite)	Carbonate (Calcite)
221, 246, 295, 405, 490, 607, 1315	Oxide (Hematite)	Oxide (Hematite)
550, 663	Oxide (Magnetite)	Oxide (Magnetite)
420, 567, 960, 1017	******	Phosphates (Apatite)
420, 480	******	Zeolite (Phillipsite)
1061	Carbonate (Hidrotalcite)	******

Table 2. Band analysis of olivine in the different outcrops on the principal Raman vibration (after Kuebler et al., 2006; Mouri and Enami, 2008)

Sample	**Band at 820 cm^{-1} (DB1)**	**Band at 850 cm^{-1} (DB2)**	**Equation 1**	**Equation 2**
Las Arenas Negras volcano				
TNFG1	821	851	Forsterite$_{85}$	Forsterite$_{80}$
TNFG1	822	848	Forsterite$_{90}$	Forsterite$_{90}$
TNFG2	821	851	Forsterite$_{80}$	Forsterite$_{80}$
TNFG2	819	849	Forsterite$_{70}$	Forsterite$_{80}$
TNFG3	821	853	Forsterite$_{90}$	Forsterite$_{85–90}$
TNFG3	821	850	Forsterite$_{70–80}$	Forsterite$_{75–80}$
Pillow lava zone				
TNF (fresh part)	821	848	Forsterite$_{80}$	Forsterite$_{80–90}$
	819	853	Forsterite$_{60–70}$	Forsterite$_{80–90}$
TNF (external part)	820	851	Forsterite$_{90}$	Forsterite$_{80–85}$
	818	847	Forsterite$_{40–60}$	Forsterite$_{60–65}$
Equation 1 (Kuebler et al., 2006)	$Fo(DB1,DB2) = -206232.988995287 + 80.190397775029\,(DB1) + 399.350231139156\,(DB2) - 0.0424363912074934\,(DB1)^2 - 0.2357973451030880\,(DB2)^2$			
Equation 2 (Mouri and Enami, 2008)	$Mg^{\#} = -610.65 + 1.3981\,(DB2) - 0.00079869\,(DB2)^2$ $Mg^{\#} = -3715.8 + 8.9889\,(DB1) - 0.0054348\,(DB1)^2$			

Table 3. Band analysis of the Raman vibration on the pyroxenic mineral from the different outcrop. The peaks have been normalized to the maximum

Position band analysis				
Sample	**Band at 1000 cm^{-1} (DB1)**	**Band at 665 cm^{-1} (DB2)**	**Band at 325 cm^{-1} (DB3)**	**Equation**
The Arenas Negras Volcano				
TNFG1 (Sample 1)	1001	664	324	Diopside
TNFG1 (Sample 2)	1002	661	321	Diopside
TNFG2 (Sample 1)	1006	663	319	Diopside
TNFG2 (Sample 2)	1003	663	324	Diopside
TNFG3 (Sample 1)	1004	664	323	Diopside
TNFG3 (Sample 1)	1002	659	320	Diopside
Pillow lavas zone				
TNF (Sample 1)	1002	665	****	Diopside
	1001	668	325	Diopside
TNF (Sample 2)	1000	667	****	Diopside
	1002	668	323	Diepside
Equation (Huang et al., 2000)	Fe(2) = 10406 – 15.649 (DB2); Fe(3) = 1415 – 4.3554 (DB3)			
FWHM band analysis				
TNFG1	22,556	19,338		
TNFG2	21,430	20,218		
TNFG3	19,890	18,341		
TNF	32,460	30,181		
TNF	25,145	23,450		

Table 4. Resume of the mineral species detected on Tenerife and the Mineral comparison with Mars. X indicates that these species were uniquely identified with the technique, while O indicates that compatible results.

Minerals	**Pillow Lavas**			**Arenas Negras Volcano**			**Reported on Mars**
	Raman	XRD	IR	Raman	XRD	IR	
Oxides							
Magnetite (Fe_3O_4)	X	X		X	X		X
Haematite (Fe_2O_3)	X	X		X	X		X
Silica (SiO_2)	X	X		X	X		X
Carbonates							
Calcite ($CaCO_3$)	X			X			X
Hydrotalcite ($Mg_6Al_2(CO_3)(OH)_{16}\cdot 4(H_2O)$)	X						
Phosphates							
Apatite ($Ca_5(PO4)_3(F,Cl,OH)$)	X			X			
Silicates							
Inosilicates							
Piroxenes							
Diopside ($MgCaSi_2O_6$)	X	X	O	X	X	O	X
Augite ($(Ca,Mg,Fe)_2(Si,Al)_2O_6$)	X	X	O	X	X	O	X
Nesosilicates							
Olivine							
Forsterite ($(Fe,Mg)_2SiO_4$)	X	X	O	X	X	O	X
Tectosilicates							
Feldspars and plagioclase		X			X		X
Anorthoclase ($(Na,K)AlSi_3O_8$)			O	X		O	
Anorthite ($CaAl_2Si_2O_8$)			O			O	
Albite($NaAlSi_3O_8$)			O	X		O	
Oligoclase and Andesine ($(Na,Ca)(Si,Al)_4O_8$)	X		O	X		O	

Labradorite ((Ca,Na)(Si,Al)$_4$O$_8$)	X		O			O	
Zeolites							X
Phillipsite ((Ca,K,Na)$_6$(Si$_{10}$Al$_6$)O$_{32}$12H$_2$O)				X			

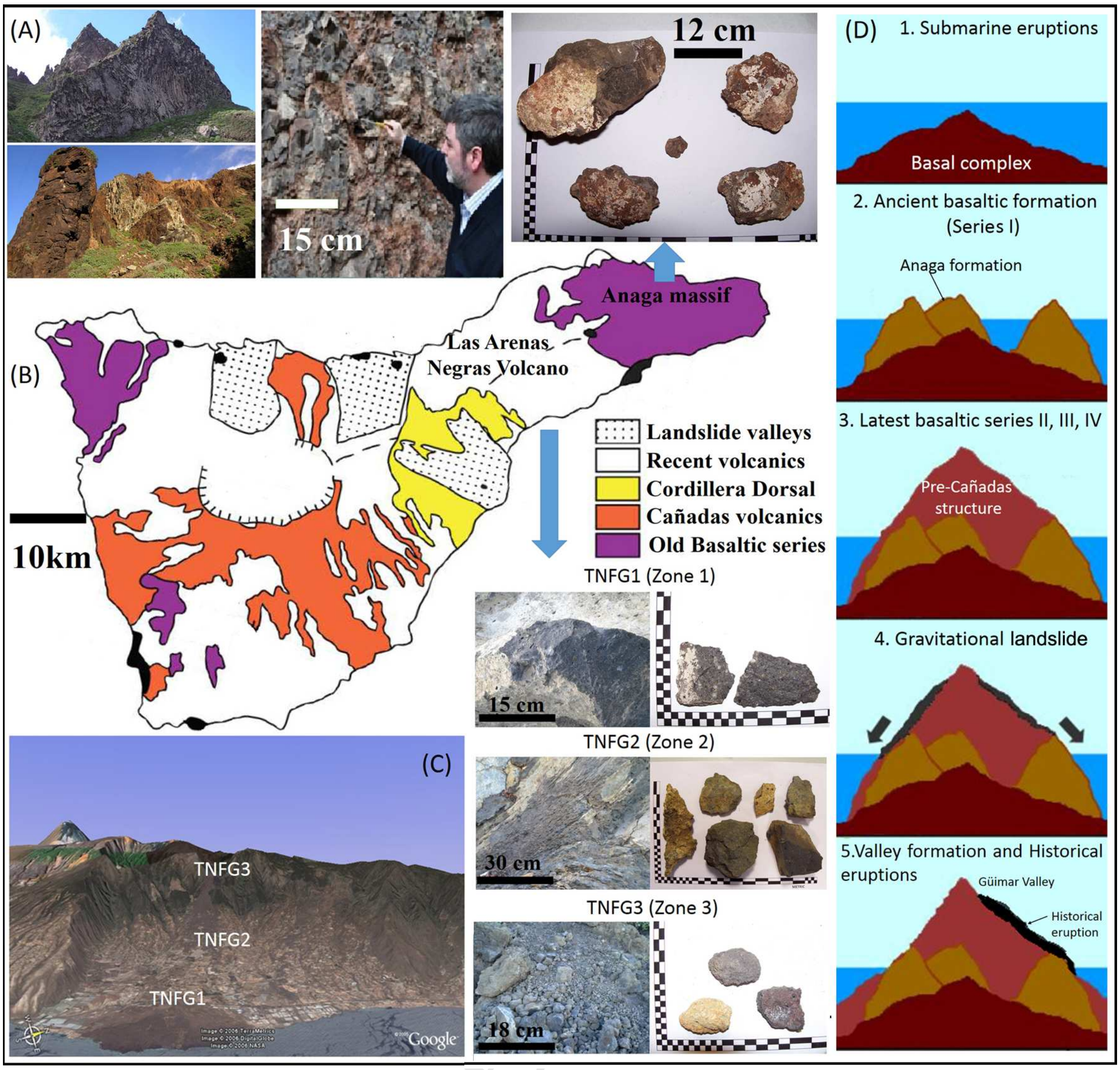

(A)
15 cm
12 cm
(B)
Anaga massif
Las Arenas
Negras Volcano
10km
Landslide valleys
Recent volcanics
Cordillera Dorsal
Cañadas volcanics
Old Basaltic series
TNFG1 (Zone 1)
15 cm
TNFG2 (Zone 2)
30 cm
TNFG3 (Zone 3)
18 cm
(C)
TNFG3
TNFG2
TNFG1
Google
(D)
1. Submarine eruptions
Basal complex
2. Ancient basaltic formation
(Series I)
Anaga formation
3. Latest basaltic series II, III, IV
Pre-Cañadas
structure
4. Gravitational landslide
5.Valley formation and Historical
eruptions
Güimar Valley
Historical
eruption

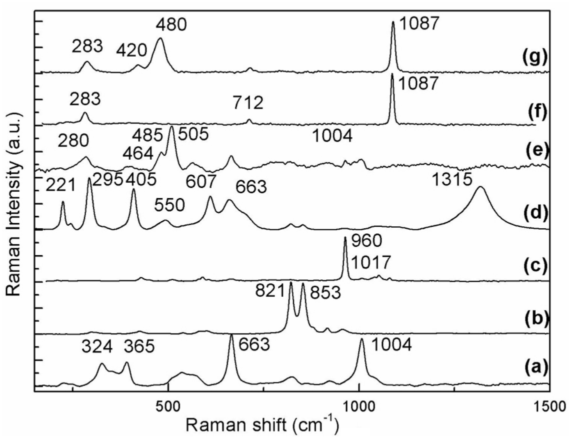

283
420
480
1087
(g)
283
712
1087
(f)
280
485
505
464
1004
(e)
221
295
405
607
663
1315
550
(d)
960
1017
(c)
821
853
(b)
324
365
663
1004
(a)
Raman Intensity (a.u.)
500
1000
1500
Raman shift (cm-1)

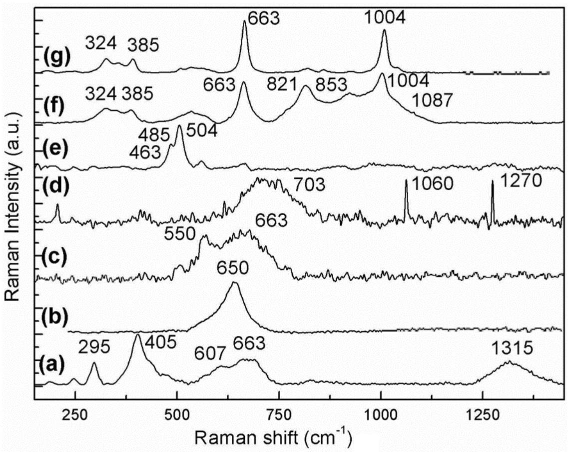

Raman Intensity (a.u.)
Raman shift (cm-1)
250
500
750
1000
1250
(g)
324
385
663
1004
(f)
324 385
663
821
853
1004
1087
(e)
485
504
463
(d)
703
1060
1270
(c)
550
663
(b)
650
(a)
295
405
607
663
1315

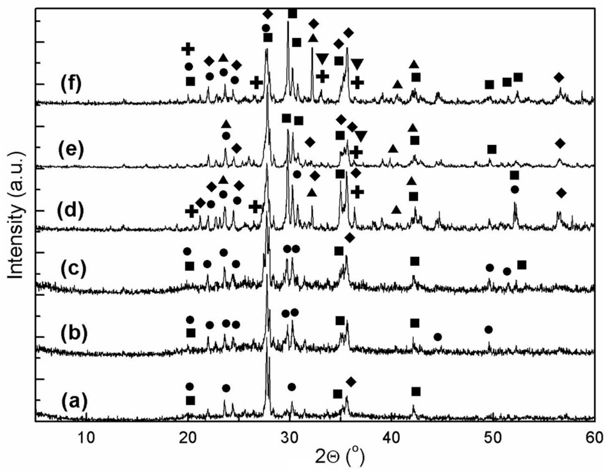

(f)
(e)
(d)
(c)
(b)
(a)
Intensity (a.u.)
10
20
30
40
50
60
2Θ (°)

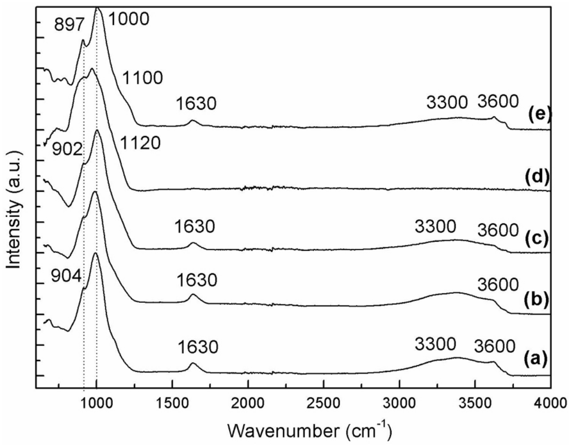

897
1000
1100
1630
3300
3600
(e)
902
1120
(d)
1630
3300
3600
(c)
904
1630
3600
(b)
1630
3300
3600
(a)
Intensity (a.u.)
1000
1500
2000
2500
3000
3500
4000
Wavenumber (cm-1)

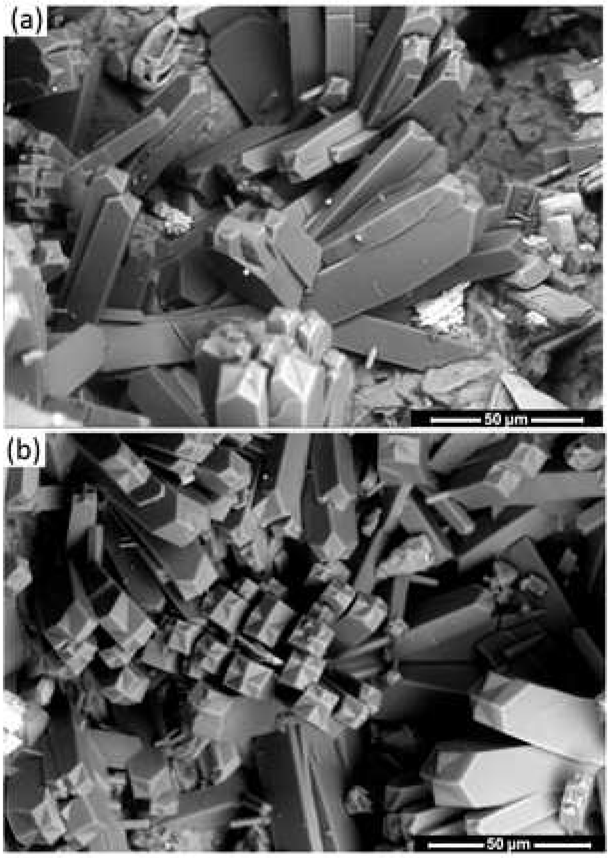
(a)
50 µm
(b)
50 µm

HIGHLIGHTS:

Tenerife eruptions as analogue for ancient Mars

Micro-Raman characterization of mineral phases

Zeolite mineral phase identified in the Arenas Negras volcano